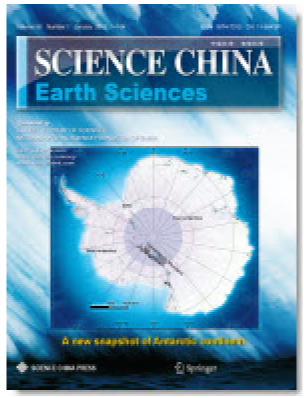

Co-varying temperatures at 200hpa over the Earth's three poles

Journal:	*SCIENCE CHINA Earth Sciences*
Manuscript ID	SCES-2020-0041.R3
Manuscript Type:	Research paper
Date Submitted by the Author:	n/a
Complete List of Authors:	Fang, keyan; Fujian Normal University, College of Geographical Sciences Zhang, Peng; University of Gothenburg, Department of Earth Sciences Chen, Jingming; Fujian Normal University, College of Geographical Sciences Chen, Deliang ; University of Gothenburg, 5Regional Climate Group, Department of Earth Sciences
Keywords:	three poles, Tibetan Plateau, Brewer-Dobson circulation, Interdecadal Pacific Oscillation, climate teleconnection
Speciality:	Climate Change, Dendrochronology

Co-varying temperatures at 200hpa over the Earth's three poles

Keyan FANG[1,2,*], Peng ZHANG[2], Jingming CHEN[1,3], Deliang CHEN[2]

1. Key Laboratory of Humid Subtropical Eco-geographical Process (Ministry of Education), College of Geographical Sciences, Fujian Normal University, Fuzhou 350007, China
2. Regional Climate Group, Department of Earth Sciences, University of Gothenburg, Box 460 S-405 30 Gothenburg, Sweden
3. Department of Geography and Program in Planning, University of Toronto, 100 St. George St., Toronto, Ontario, Canada

Abstract

The Earth's three poles, the North Pole, South Pole, and Third Pole (i.e., the Tibetan Plateau and its surroundings), hold the largest amount of fresh water on Earth as glaciers, sea ice, and snow. They are sensitive to climate change. However, the linkages between climate variations of the three poles, particularly between the South Pole and Third Pole, remain largely unknown. The temperatures at 200hpa over the three poles are the highest in the summer and are less affected by surface conditions, which could reflect large-scale dynamic linkages. Temperatures at 200hpa peak the three poles during their respective hemispheric summer and exhibit in-phase variations on interdecadal timescales (10–100 years). The 200hpa temperatures over the North Pole and South Pole were significantly correlated with the Brewer–Dobson circulation (BDC), which transports stratospheric ozone poleward, heating the air at 200hpa. Tropopause warming over the Third Pole was found to enhance the poleward BDC, particularly to the South Pole, linking the Third Pole's climate to the other two poles. Additionally, the Interdecadal Pacific Oscillation (IPO) also exhibits links with the 200hpa temperatures of the three poles.

Keywords: three poles; Tibetan Plateau; Brewer-Dobson circulation; Interdecadal Pacific Oscillation; climate teleconnection

1. Introduction

The three poles, i.e., the North Pole and South Pole and the so-called Third Pole that consists of the Tibetan Plateau and its surroundings, have the largest amount of ice volumes on Earth. They are especially sensitive to global climate change. For example, warming in recent decades is more pronounced at the North Pole because of the so-called Arctic amplification (Serreze and Barry, 2011) and at the Third Pole (Chen et al., 2015; Yao et al., 2018) because of an elevation-dependent warming pattern (Pepin et al., 2015). Conversely, a significant cooling trend was observed at the South Pole during the first half of the 20th century, which has reversed in recent decades (PAGES 2k Consortium, 2013; Wang et al., 2015). In addition, the three poles cause global climate anomalies through local feedbacks and large-scale teleconnections (Chen et al., 2015; Stocker et al., 2013; Yao et al., 2018). Currently, the scientific community is starting to recognize the importance of unified research on the three poles in order to reveal their teleconnections.

Numerous studies have revealed a see-saw climate pattern between the North Pole and South Pole *via* thermohaline circulation (Blunier and Brook, 2001; Chylek et al., 2010; Marino et al., 2015; Wang et al., 2015). Previous studies have also revealed climate linkages between the North Pole and Third Pole (Zhang et al., 2019) and between the South Pole and the eastern Asian climate *via* the Asian–Australian summer monsoon (Chen et al., 2016; Fang et al., 2018a; Fang et al., 2015). There is a lack of a clear understanding of climate linkages among the three poles, particularly between the South Pole and the Third Pole. Although a unified physical framework has been employed to quantify the strengths of various physical mechanisms behind surface temperature changes at the three poles (Gao et al., 2019), no study to date has looked at the linkages of climate changes among the three poles simultaneously.

Existing investigations have largely focused on the linkages between the surface climates of the three poles. This study focuses on the co-variability between the temperatures of the three poles at 200hpa, which are not only significantly impacted by surface conditions but also closely related to dynamical atmospheric processes (Ding and Wang, 2005). Thus, the 200hpa temperature may reflect large-scale climate linkages among the three poles.

2. Data and methods

2.1 Data

This study employed monthly 200hpa temperature from a reanalysis dataset developed by the National Center for Environmental Predictions-National Center for Atmospheric Research (NCEP-NCAR) spanning from 1948 to the present (Kalnay et al., 1996; Kistler et al., 2001). This dataset was derived through data assimilation from both modelings and measurements. For comparison, we also employed reanalysis datasets of ERA-Interim (1979–present), which was developed by the European Centre for Medium-Range Weather Forecasts (ECMWF), and the Modern Era Retrospective-Analysis for Research and Applications (MERRA; 1979–2016), which was produced by the Global Modeling and Assimilation Office of the National Aeronautics and Space Administration (NASA) (Rienecker et al., 2011). We focused on the NCEP-NCAR reanalysis dataset as it shows similar results to the other datasets and has a longer duration.

We used 1^{o} gridded sea surface temperature (SST) datasets spanning from 1871 onward from the Hadley Centre Global Sea Ice and Sea Surface Temperature dataset (HadISST) (Kennedy et al., 2011). The SST data from 1982 onward were based on the data from the Met Office Marine Data Bank (MDB) and the Global Telecommunications System (GTS). In periods with no MDB data, the dataset was derived from monthly median SSTs for the period 1871–1995 obtained from the International Comprehensive Ocean-Atmosphere Data Set(ICOADS). This study used the Multi-sensor Reanalysis version 2 global ozone column dataset (1970–present), which was developed by the Royal Netherlands Meteorological Institute (van der et al., 2015). The early data from 1970 were based only on one instrument (BUV) on the Nimbus-4 satellite. Contrarily, data since 1978 were based on two instruments (SBUV and TOMS) on the Nimbus-7 satellite, which were more robust (van der et al., 2015). This study only used high-quality data from after 1978.

We compiled networks of annually resolved climate-sensitive proxies for the Third Pole

(20–45°N; 45–105°E). These proxies spanno later than 1800 and no earlier than 1980 and were mainly derived from the PAGES 2k project (PAGES 2k Consortium, 2013) and other large-scale climate reconstructions (Fang et al., 2018b) from the National Climate Data Center (NCDC, www.ncdc.noaa.gov/data-access/paleoclimatology-data). The network consists of 202 proxies, most of which were derived from tree rings (196), ice cores (5), and composite records (1). Details on proxy data processing are provided in the Appendix.

2.2 Methods

We used wavelet coherence (WTC) methods to evaluate the time-varying correlations between time series on different timescales. The WTC method is based on wavelet analyses to transform time series data into components of different timescales and then calculate local correlations (Grinsted et al., 2004; Torrence and Compo, 1998). We employed the first principal component (PC1) of the selected proxies in order to reconstruct 200hpa temperature for the Third Pole. To ensure a sufficiently long common calibration period for reconstruction, we used the regularized expectation maximization (RegEM) method (Fang et al., 2018a; Mann et al., 2009; Shi et al., 2015) to fill the missing proxy values in the instrumental period. By doing so, we infilled proxy data at the Third Pole to achieve a common period from 1948 to 1996. More details on our reconstruction methods are provided in the Appendix.

The monthly net mass fluxes from the troposphere to the stratosphere over 30°S–30°N were generated using mass stream functions that were calculated based on atmospheric temperature and meridional wind velocity data derived from the NCEP-NCAR daily reanalysis dataset (Kalnay et al., 1996; Kistler et al., 2001). We defined the monthly tropopause as the lowest pressure level wherein the lapse rate decreases to 2K/km or less, provided that the average lapse rate between this level and all the higher levels within 2km does not exceed 2K. We calculated the monthly tropopause using the same atmospheric temperature data as those used for the mass flux calculations.

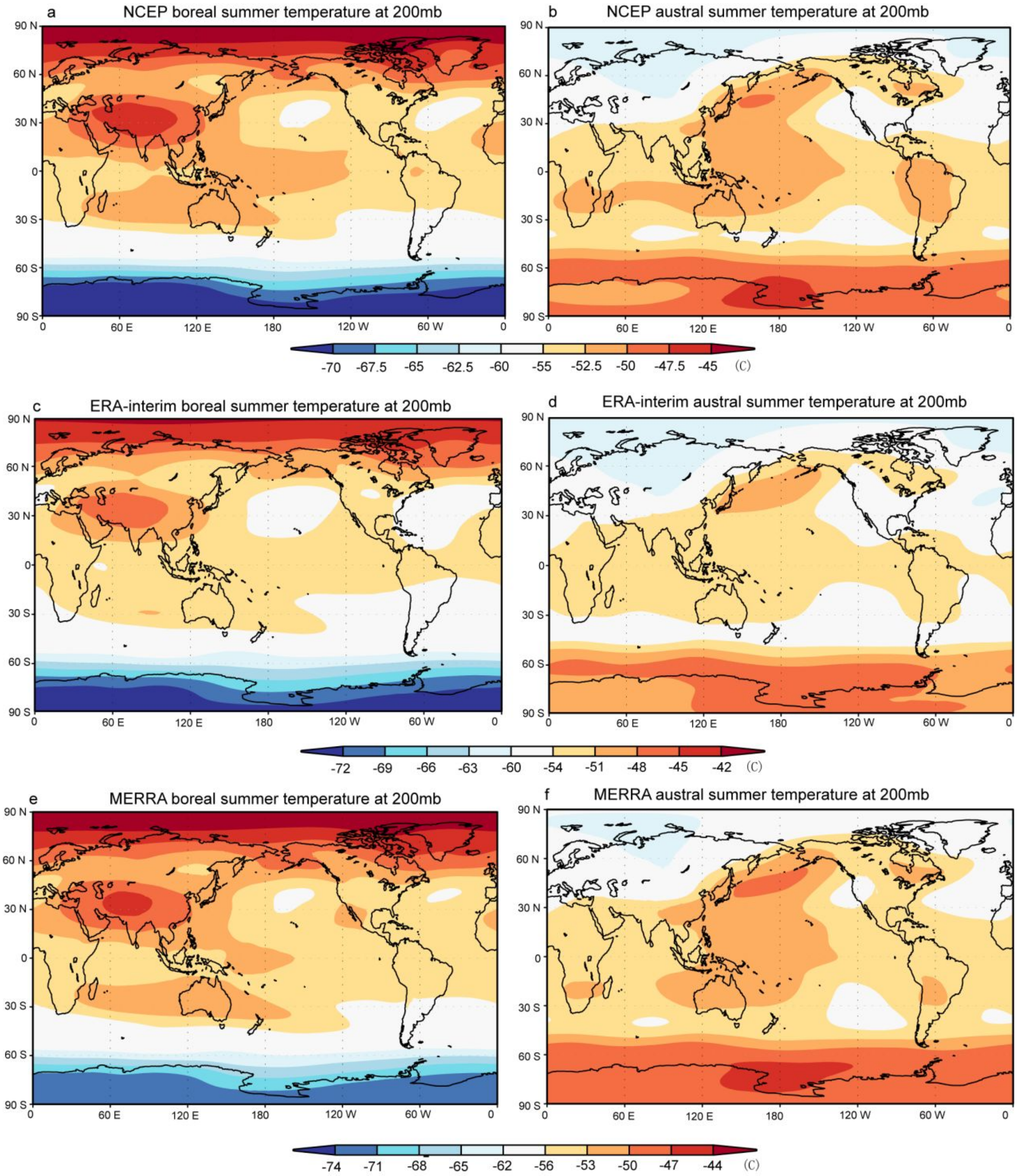

Fig. 1. Mean temperature at 200hpa from 1948 to 2018 in the (a, c, and e) boreal (June–August) and (b, d, and f) austral summers (December–February) derived from the NCEP, ERA-Interim, and MERRA reanalysis datasets.

3 Results and Discussion

3.1 Co-varying temperatures at 200hpa and their linkages to the BDC

3.1.1 Co-varying temperatures at 200hpa at the three poles

Temperatures at the 200hpa peak during the respective hemispheric summers of the three poles are the coldest during their respective hemispheric winters (Fig. 1); however, this is not clear for temperatures below 200hpa (Fig. S1). Temperatures at 200hpa are in the tropopause at the Third Pole and in the stratosphere at the North Pole and South Pole. This is ideal for studying linkages among the tropopause, stratosphere, and surface climates of the three poles. The North Pole and South Pole have the longest heating durations in the boreal and austral summers, respectively. In addition, heat transported from the tropics to the North Pole and South Pole is strengthened during the respective hemispheric summers (Boos and Kuang, 2010; Rao et al., 2019; Zhao et al., 2011). Due to the high elevations, the Third Pole strongly heats the upper troposphere air mass, thus causing the Third Pole to be one of the warmest areas at 200hpa during the boreal summer (Chen et al., 2015; Wu et al., 2007). We averaged the 200hpa temperatures to generate time series data for the North Pole (60–90°N, 0–360°E), South Pole (60–90°S, 0–360°E), and Third Pole (25–40°N, 50–100°E) during their respective hemispheric summers. The 200hpa temperatures exhibited the strongest variability at the South Pole, with the 200hpa temperature variations three times larger than at the North Pole (Fig. 2a). In general, the 200hpa temperatures of the three poles closely match the interdecadal timescales (10–100 years) during their hemispheric summers, particularly for periodicities of more than ~20 years (Fig. 2 and S2).

The 200hpa temperatures at the North Pole and South Pole are in the stratosphere, and the energy absorbed by the ozone layer is a key source of stratosphere heating (Lu et al., 2019). It is thus readily understood that there are significant positive correlations between the 200hpa temperatures and the *in situ* ozone column concentrations at the North Pole and South Poles (Fig. 3a and 3b). Contrarily, the 200hpa temperatures at the North Pole showed almost no significant correlation with the *in situ* ozone concentration (Fig. 3c).

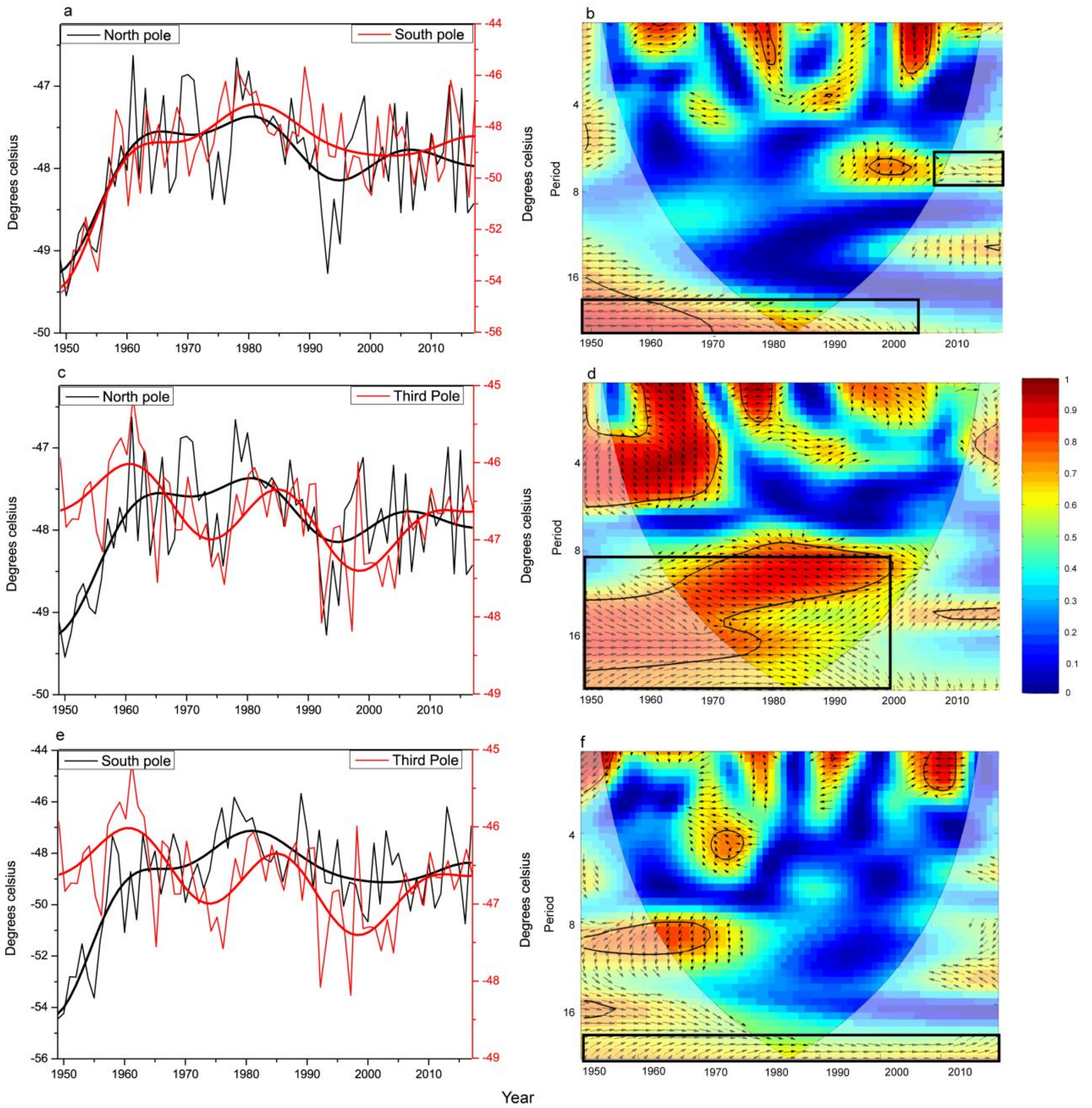

Fig. 2. Comparisons of the 200hpa temperatures and wavelet coherence (WTC) between the (a and b) North Pole and South Pole, the (c and d) North Pole and Third Pole, and the (e and f) South Pole and Third Pole. Significant correlations are indicated by contours, and the arrows pointing left (right) indicate the in-phase (anti-phase) correlations. Temperatures were calculated during the boreal and austral summers.

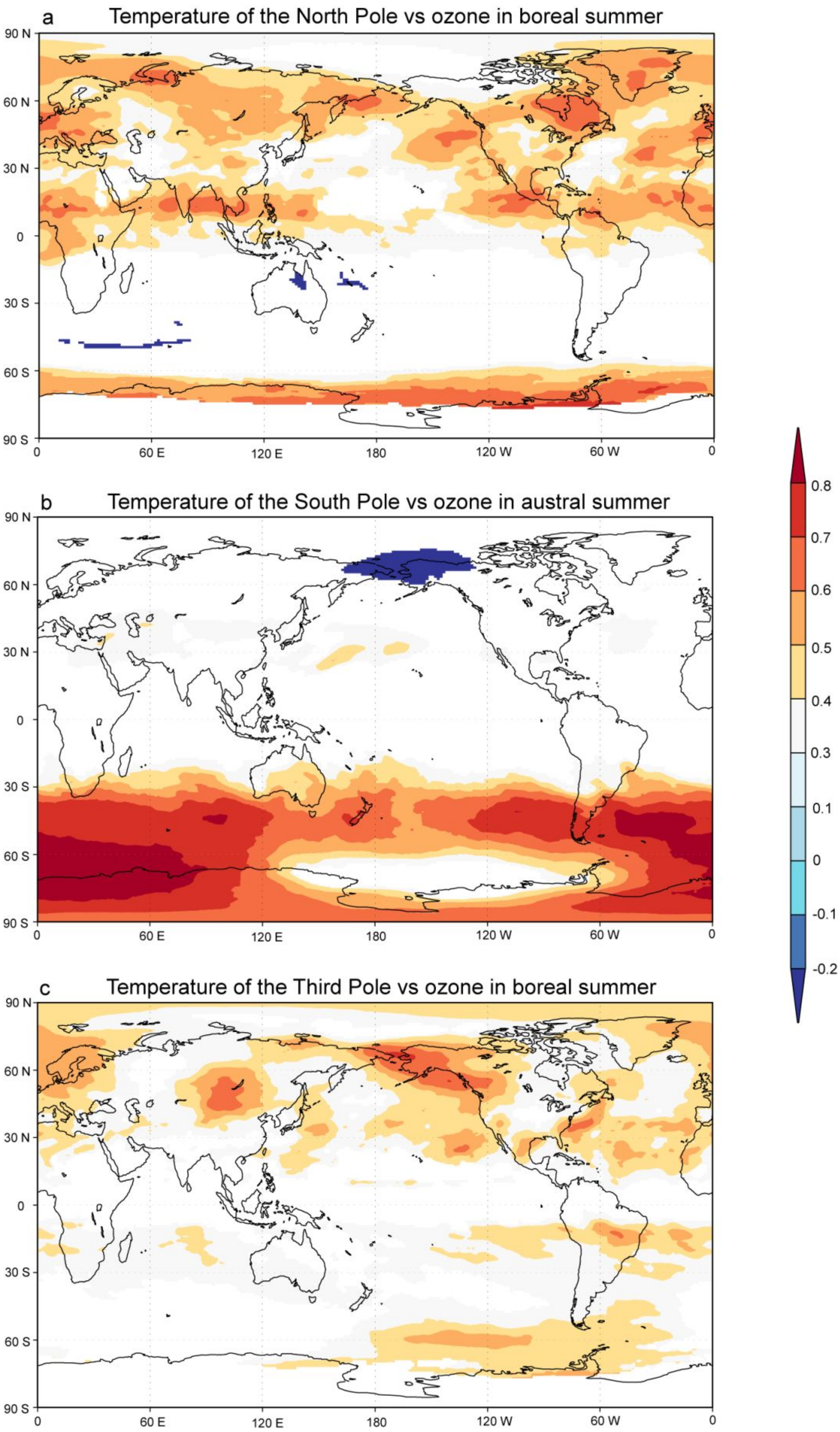

Fig. 3. Map of the correlations between the (a) 200hpa temperatures and mean ozone concentration at the North Pole in boreal summer (June–August), (b) 200hpa temperatures and ozone concentration at the South Pole in austral summer (December–February), and (c)

200hpa temperatures and ozone concentration at the Third Pole in boreal summer.

3.1.2 Links to the BDC

Ozone is mainly transported from the tropics to the North Pole and South Pole by the Brewer–Dobson circulation (BDC), which ascends from the tropical tropopause to the stratosphere and descends back to the troposphere at the North Pole and South Pole (Brewer, 1945; Dobson, 1956). We calculated the monthly troposphere-to-stratosphere mass fluxes over the tropics (30°S–30°N) as BDC intensity indicators, which were then compared with the 200hpa temperatures of the three poles (Fig. 4). There were moderately high correlations between the BDC intensity in the northern (southern) hemispheres and the 200hpa temperatures at the North (South) Pole (Fig. 4a and 4b). Thus, it is reasonable for an enhanced BDC, and its associated higher poleward ozone transport, to cause warming at 200hpa.

The strongest correlations were observed between the 200hpa temperatures at the Third Pole and the BDC to the Southern Hemisphere on interdecadal timescales (Fig. 4c). Boreal summer heating over the Third Pole leads to a warmer tropopause than over the neighboring areas (Zhao et al., 2011), which can drive a greater air mass from the tropopause to the stratosphere over the Third Pole. The heating at the Third Pole and its effects on large-scale circulations are concentrated in its southern part near the Himalayas (Boos and Kuang, 2010), which falls within the area of troposphere-to-stratosphere mass transport. The BDC is stronger in winter due to enhanced wintertime Rossby and gravity waves (Holton et al., 1995); therefore, boreal summer mass transport tends to go to the Southern Hemisphere, as it is winter in the Southern Hemisphere.

Given the strong correlations between the ozone concentration and 200hpa temperatures over the South Pole, we consider the South Pole and Third Pole to be linked *via* the BDC from the Third Pole to the South Pole. The 200hpa temperatures over the Third Pole are closely linked to the Australian–Asian summer monsoon (Tang et al., 2011; Wu et al., 2007). We hypothesize the presence of a circulation from the surface in the Southern Hemisphere to the tropopause of the southern portion of the Third Pole, which is driven by the Australian–Asian summer monsoon and then returns to the Southern Hemisphere from the stratosphere to the troposphere over the South Pole. Additionally, an increased ozone concentration over the South Pole often corresponds to a decreased Southern Annual Mode (SAM), leading to weakened westerlies over the Southern Hemisphere (Sexton, 2001). Weakened westerlies can be associated with a weakened Peru Current and an El Niño condition (Fang et al., 2015).

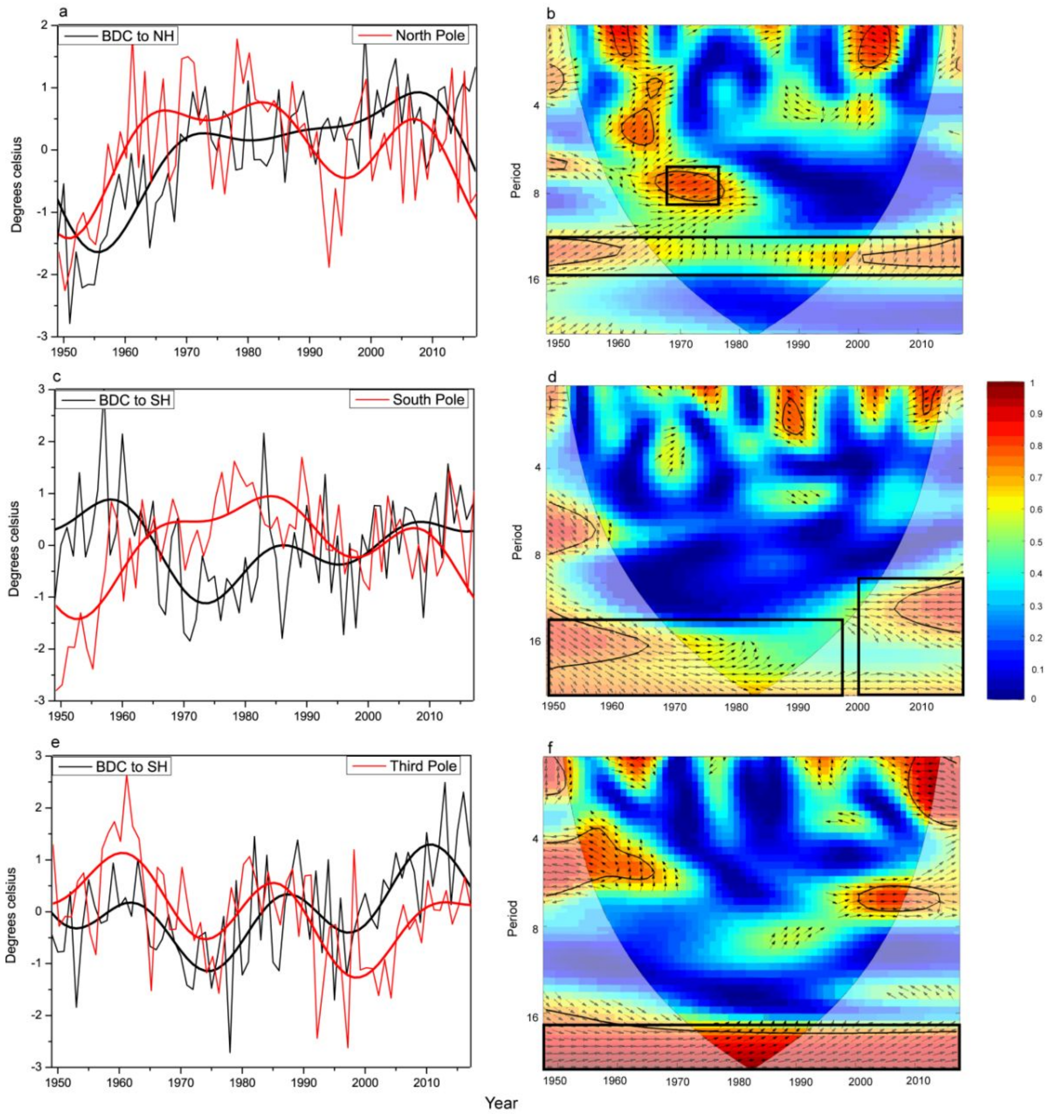

Fig. 4. Temperature comparisons and wavelet coherence (WTC) for the z-scored pairs of (a and b) North Pole boreal summer 200hpa temperature and mass transport from the tropics (30^{o}S–30^{o}N) by the Brewer–Dobson Circulation (BDC) to the Northern Hemisphere in boreal spring and summer (Mar–August), (c and d) South Pole austral summer 200hpa temperature and mass transport by BDC to the Southern Hemisphere in austral spring and summer (September–February), and (e and f) Third Pole boreal summer 200hpa temperature and

annual mass transport by BDC to the Southern Hemisphere. As BDC is a relatively slow process, correlations with BDC intensity included 3 months before summer. Contours in the WTC maps (b, d, and f) indicate the boundary with significant correlations, and the arrows pointing left (right) indicate in-phase (anti-phase) correlations. All the data for calculations were normalized to have a zero mean and a standard deviation of 1.

3.2 The Interdecadal Pacific Oscillation and co-varying 200hpa temperatures

3.2.1 Links to the Interdecadal Pacific Oscillation

We calculated the correlations between the co-varying 200hpa temperatures of the three poles and SST in concurrent summer and previous winter, as SST often plays key roles in climate variation on interdecadal timescales. Temperatures at the North Pole (Fig. 5a and 5b), South Pole (Fig. 5c and 5d), and Third Pole (Fig. 5e and 5f) exhibited significant positive correlations with SST in the eastern equatorial Pacific Ocean and negative correlations with SST in mid-latitudes in the northern and southern Pacific Oceans. This is a pattern resembling the Interdecadal Pacific Oscillation (IPO) (Henley et al., 2015). This IPO-like correlation pattern is particularly strong for the correlations of the Third Pole (Fig. 5e and 5f) with 200hpa temperature. The correlations with annual SST also exhibit IPO-like patterns (Fig. S3 and S4), particularly for the South Pole (Fig. S3b). These results suggest positive associations between the IPO and 200hpa temperatures at the three poles.

As a dominant Pacific SST pattern, the IPO plays a key role in shaping North and South Pole co-variability that mainly exists on interdecadal timescales. The IPO may modulate the temperatures of the three poles *via* the Hadley circulation and BDC. The Hadley circulation is a key atmospheric feature that transports heat from the tropics to the North Pole and South Pole. Previous studies revealed an enhanced rising limb of the Hadley circulation in response to a positive phase of the IPO (Fu et al., 2006; Seidel et al., 2007). This can cause warm conditions at 200hpa over the North Pole and South Pole. In addition, previous studies revealed positive correlations between the strength of the eastern equatorial Pacific SST and BDC (Rao et al., 2019). An enhanced BDC during the warm phase of the IPO can be associated with increased ozone concentration, which can cause warm 200hpa temperatures

(Lu et al., 2019).

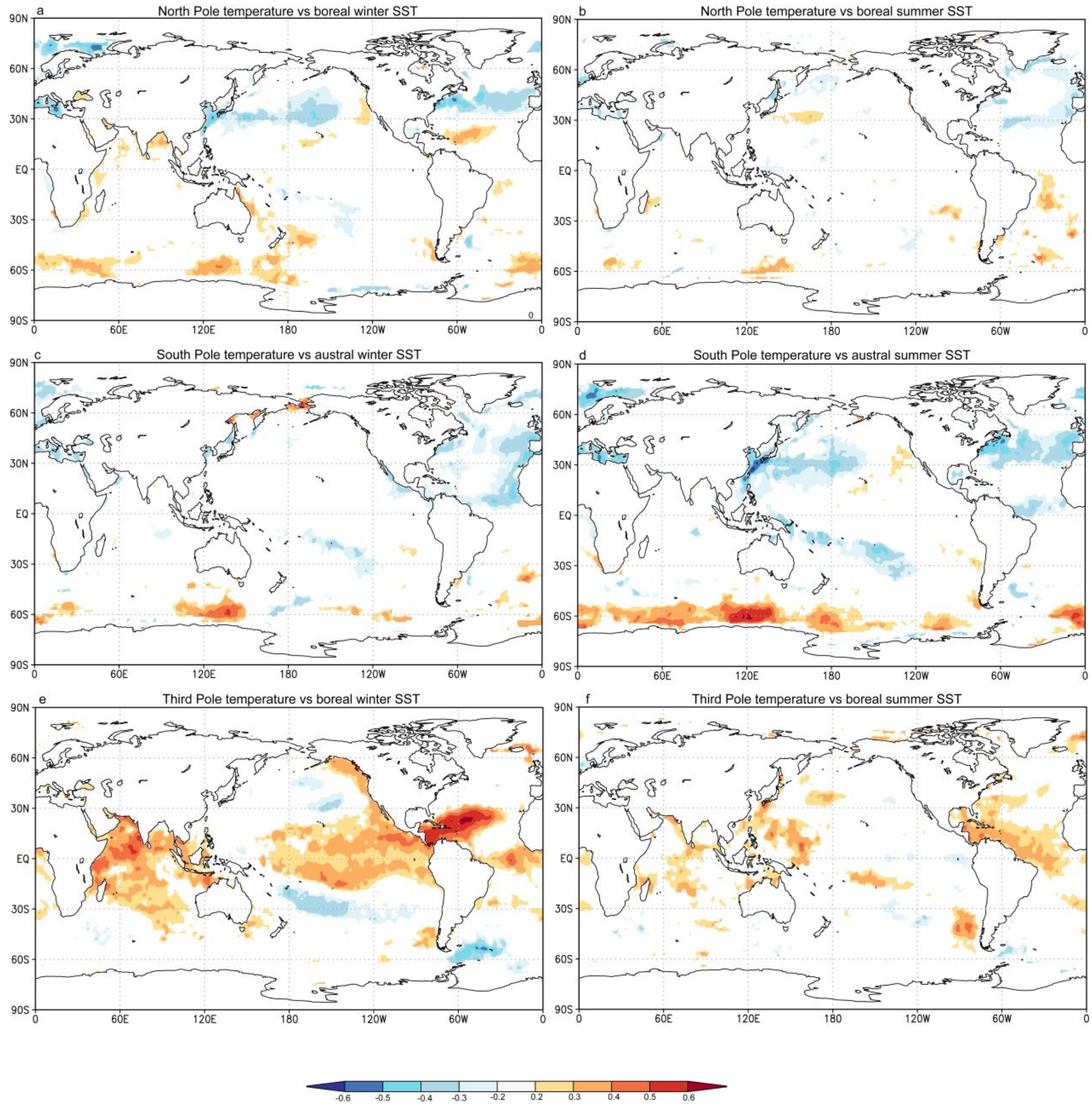

Fig. 5. Map of the correlations between the North Pole boreal summer 200hpa temperature and sea surface temperature (SST) in the (a) previous boreal winter and (b) current boreal summer, between the South Pole 200hpa temperature and SST in (c) the previous austral winter and (d) current austral summer, and between the Third Pole 200hpa temperature and SST in the (e) previous boreal winter and (f) current boreal summer during their common period (1948–2017).

3.2.2 Coupled changes of the IPO and temperature at the Third Pole

The above results suggest that heating at low latitudes, particularly at the Third Pole and in the tropical Pacific, as represented by the IPO, play key roles in modulating the 200hpa temperatures of the North Pole and South Pole. Previous studies have revealed that heating at the Third Pole can enhance the South Asian High over its tropopause, which was a key process of Indian summer monsoon dynamics (Wei et al., 2015). The surface and tropopause climates of the Third Pole are physically linked in boreal summer; thus, we further reconstructed the 200hpa temperatures for the Third Pole using surface tree ring and ice core data (Fig. S5a and Table S1). The 200hpa temperatures at the Third Pole were reconstructed back to 1678, with the proxies explaining 30.9% of the variance in the reanalysis data (Fig. S5b). More details are presented in the Appendix. The reconstructed temperatures were compared with the existing reconstruction of tropical Pacific SST modes in order to investigate their linkages over long timescales.

For comparisons with the Third Pole temperature reconstruction, we only selected robust climate reconstructions that can be verified by other reconstructions from independent proxies. We did not find such an IPO reconstruction that met this requirement. Instead, we employed reconstructions with robust interdecadal variations from the El Niño-Southern Oscillation (ENSO) (Fang et al., 2019; Wilson et al., 2010) (Fig. 6a) and the SAM (Villalba et al., 2012) (Fig. 6b). Previous studies revealed coherent multi-decadal climate variability in the areas of the Pacific Ocean, which is defined as the Multi-decadal Pacific Oscillation (MPO) (Fang et al., 2018b). Moreover, we compared the MPO with the reconstructed 200hpa temperature over the Third Pole. ENSO, IPO, and MPO are strongly correlated on different timescales (Fang et al., 2019), and the major differences are their dominant timescales: interannual (ENSO), interdecadal (IPO), and multi-decadal (MPO). The MPO covers the entire Pacific Ocean, differing from the Pacific Multi-decadal Variability (PMV) (Zhong et al., 2008) and Pacific Multi-decadal Oscillation (PMO) (Steinman et al., 2015), which focus on the North Pacific Ocean.

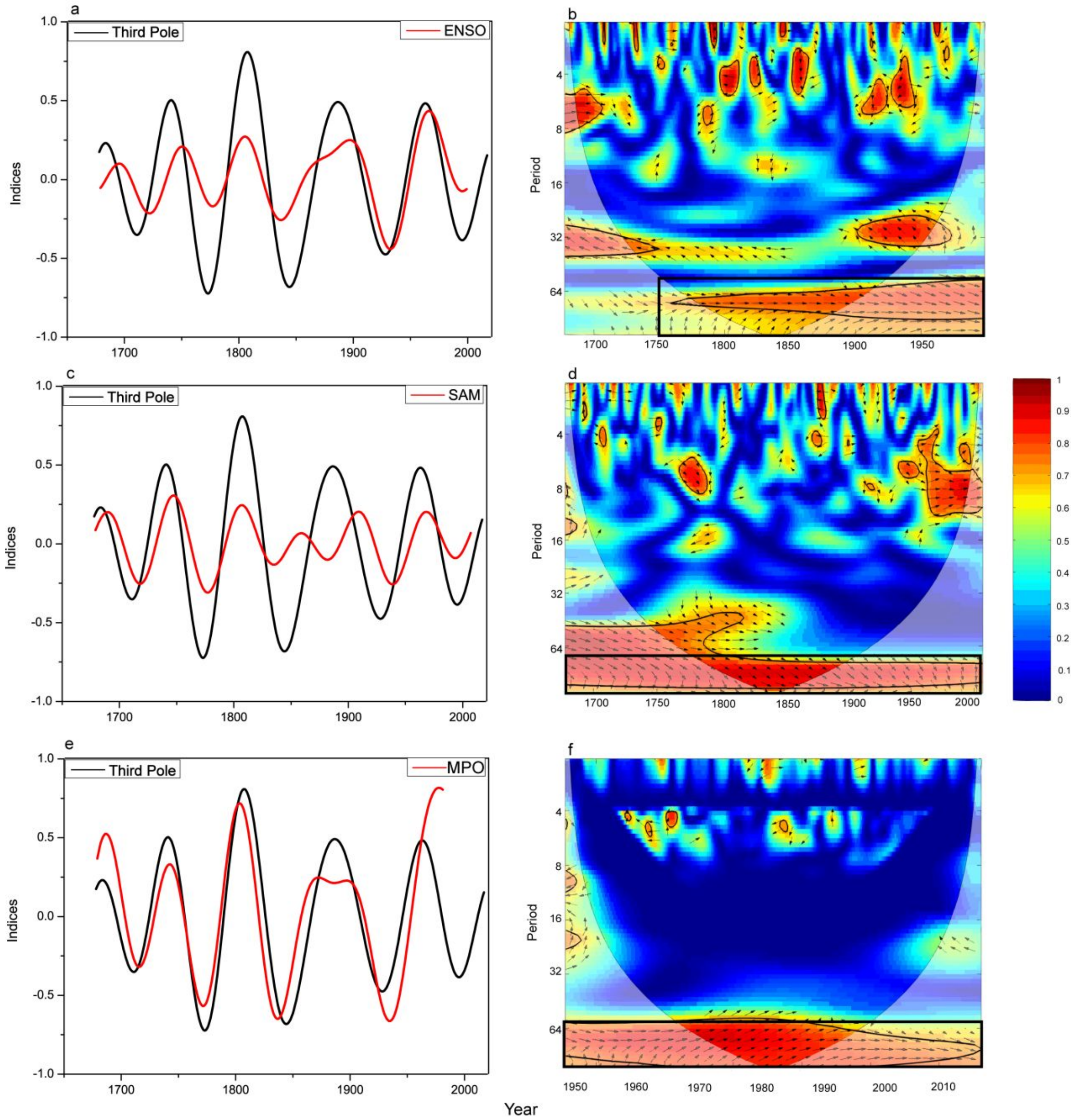

Fig. 6. Comparisons and wavelet coherence (WTC) between the reconstructions of the Third Pole boreal summer 200hpa temperature and the (a and b) reconstructed El Niño-Southern Oscillation (ENSO), the (c and d) reconstructed Southern Annual Mode (SAM), and the (e and f) reconstructed Multi-decadal Pacific Oscillation (MPO). The comparisons were conducted on multi-decadal ($f < 0.02$) timescales because that was the timescale in which the correlations were the strongest. Note that the ENSO and SAM reconstructions have no overlapping proxies with the Third Pole reconstruction, whereas the MPO reconstruction shares common proxy data in the Tibetan Plateau. Additionally, the MPO reconstruction only contains multi-decadal variability, whereas the ENSO and SAM reconstructions contain variability on different timescales.

As presented in Fig. 6, the 200hpa temperatures exhibited close matches with the reconstructed ENSO, MPO, and SAM only on multi-decadal timescales (more than ~50 years). These close matches suggest that the warming of the Third Pole and Pacific Ocean appear to be coupled. Heating at 200hpa over the Third Pole may be a factor that distributes multi-decadal climate signals to the entire Pacific region, causing the previously revealed large-scale climate co-variability of the Pacific Ocean (Fang et al., 2018b). However, we did not find strong co-variability between the reconstructed 200hpa temperature over the Third Pole and the Atlantic Multi-decadal Oscillation (AMO) reconstruction (Fig. S6).

Modeling studies have suggested a warmer eastern equatorial Pacific SST under anthropogenically forced warming at present than under the naturally forced Medieval Climate Anomaly (MCA) period (Liu et al., 2013). A warmer eastern equatorial Pacific SST can be associated with enhanced poleward heat transport, which may partially contribute to the more conspicuous warming over the North Pole. Unlike the current warming that is currently most intense over the North Pole (Serreze and Barry, 2011), the North Atlantic was found to be warmer than the North Pole during the MCA (950–1250) (Mann et al., 2009; PAGES 2k Consortium, 2013; Stocker et al., 2013). Moreover, the elevation-dependent warming pattern over the Third Pole (Pepin et al., 2015) may contribute to the current warming of the South Pole, which is opposite of the long-term cooling *via* enhanced BDC (PAGES 2k Consortium, 2013; Wang et al., 2015).

4. Conclusions

We found that 200hpa temperatures are the highest during the summer over all the three poles. Moreover, they exhibited co-variability on interdecadal timescales. We also found that the 200hpa warming over the Third Pole strengthens the poleward BDC, particularly to the South Pole. An enhanced BDC increases poleward ozone transport, thus causing warming at the other two poles, particularly at the South Pole. Previous studies found that BDC transports warming from low latitudes to the North Pole and South Pole, and our results suggest that warming at the Third Pole may be a key part of such linkages. We suggested possible mechanisms linking the 200hpa temperature to surface climate *via* the Australian–Asian summer monsoon and the IPO, which requires further modeling studies. Our study suggests the need to consider the climate teleconnection from the surface climate to the tropopause and stratospheric climate for all three poles.

Acknowledgments

The authors acknowledge those who contributed their proxy and reanalysis data to make this study possible. This study was funded by the National Science Foundation of China (41822101, 41888101, 41971022 and 41772180), Strategic Priority Research Program of Chinese Academy of Sciences (XDB26020000 and XDA20060401), the State Administration of Foreign Experts Affairs of China (GS20190157002), fellowship for the National Youth Talent Support Program of China (Ten Thousand People Plan), Youth Talent Program of Fujian province, and the innovation team project (IRTL1705). Support from the Swedish MERGE project is also acknowledged.

REFERENCES

Blunier T, Brook E J. 2001. Timing of millennial-scale climate change in Antarctica and Greenland during the last glacial period. Science, 291: 109-112

Boos W R, Kuang Z. 2010. Dominant control of the South Asian monsoon by orographic insulation versus plateau heating. Nature, 463: 218-222

Brewer A W. 1945. Evidence for a world circulation provided by measurements of helium and water vapor distribution in the stratosphere. Q J R Meteorol Soc, 75: 351-363

Chen D, Xu B, Yao T, Guo Z, Cui P, Chen F, Zhang R, Zhang X, Zhang Y, Fan J. 2015. Assessment of past present and future environmental changes on the Tibetan. Plateau Chin Sci Bull, 60: 3025-3035

Chen S, Wang Y, Cheng H, Edwards R L, Wang X, Kong X, Liu D. 2016. Strong coupling of Asian Monsoon and Antarctic climates on sub-orbital timescales. Sci Rep, 6: 32995, doi: 3291031038/srep32995

Chylek P, Folland C K, Lesins G, Dubey M K. 2010. Twentieth century bipolar seesaw of the Arctic and Antarctic surface air temperatures. Geophys Res Lett, 37, doi: 101029/2010GL042793

Ding Q, Wang B. 2005. Circumglobal Teleconnection in the Northern Hemisphere Summer. J Clim, 18: 3483-3505

Dobson G M B. 1956. Origin and Distribution of the Polyatomic Molecules in the Atmosphere Procroysoclonda. Proc Roy Soc Lond A, 236: 187-193

Fang K, Chen D, Guo Z, Zhao Y, Frank D, He M, Zhou F, Shi F, Seppä H, Zhang P. 2019. An interdecadal climate dipole between Northeast Asia and Antarctica over the past five centuries. Clim Dyn, 52: 765-775

Fang K, Chen D, Ilvonen L, Pasanen L, Holmström L, Seppä H, Huang G, Ou T, Linderholm H. 2019. Oceanic and atmospheric modes in the Pacific and Atlantic Oceans since the Little Ice Age (LIA): towards a synthesis. Quat Sci Rev, 215: 293-307

Fang K, Cook E, Guo Z, Chen D, Ou T, Frank D, Zhao Y. 2018. Synchronous multi-decadal tree-ring patterns of the Pacific areas reveal dynamics of the

Interdecadal Pacific Oscillation (IPO) since 1567. Environ Res Lett, doi: 101088/1748-9326/aa9f74

Fang K, Seppä H, Chen D. 2015. Interdecadal hydroclimate teleconnections between Asia and North America over the past 600 years. Clim Dyn, 7-8: 1777-1787

Fu Q, Johanson C M, Wallace J M, Reichler T. 2006. Enhanced mid-latitude tropospheric warming in satellite measurements. Science, 312: 1179

Gao K, Duan A, Chen D, Wu G. 2019. Surface energy budget diagnosis reveals possible mechanism for the different warming rate among Earth's three poles in recent decades. Sci Bull, doi: 101016/jscib201910061023

Grinsted A, Moore J C, Jevrejeva S. 2004. Application of the cross wavelet transform and wavelet coherence to geophysical time series. Nonlinear Process Geophys, 11: 561-566

Henley B J, Gergis J, Karoly D J, Power S, Kennedy J, Folland C K. 2015. A tripole index for the interdecadal Pacific oscillation. Clim Dyn, 45: 3077-3090

Holton J R, Haynes P H, Mcintyre M E, Douglass A R, Rood R B, Pfister L. 1995. Stratosphere-troposphere exchange. Rev Geophys, 33: 403-439

Kalnay E, Kanamitsu M, Kistler R, Collins W, Deaven D, Gandin L, Iredell M, Sana S, White G, Woollen J. 1996. The NCEP/NCAR 40-Year Reanalysis Project. Bull Amer Meteorol Soc, 77: 437-471

Kennedy J, Rayner N, Smith R, Parker D, Saunby M. 2011. Reassessing biases and other uncertainties in sea surface temperature observations measured *in situ* since 1850: 1 Measurement and sampling uncertainties. J Geophys Res-Atmos, 116

Kistler R, Kalnay E, Collins W, Saha S, White G, Woollen J, Chelliah M , Ebisuzaki W, Kanamitsu M, Kousky V. 2001. The NCEP-NCAR 50-year reanalysis: Monthly means CD-ROM and documentation. Bull Amer Meteorol Soc, 82: 247-268

Liu J, Wang B, Cane M A, Yim S Y, Lee J Y. 2013. Divergent global precipitation changes induced by natural versus anthropogenic forcing. Nature, 493: 656-659

Lu X, Zhang L, Zhao Y, Jacob D J, Hu Y, Hud L, Gao M, Liu X, Petropavlovskikh I, McClure-Begley A, Querel R. 2019. Surface and tropospheric ozone trends in the Southern Hemisphere since 1990: possible linkages to poleward expansion of the Hadley circulation. Sci Bull, 64: 400-409

Mann M E, Zhang Z, Rutherford S, Bradley R S, Hughes M K, Shindell D, Ammann C, Faluvegi G, Ni F. 2009. Global signatures and dynamical origins of the Little Ice Age and Medieval Climate Anomaly. Science, 326: 1256-1260

Marino G, Rohling E, Rodríguez-Sanz L, Grant K, Heslop D, Roberts A, Stanford J, Yu J. 2015. Bipolar seesaw control on last interglacial sea level. Nature, 522: 197-201

PAGES 2k Consortium. 2013. Continental-scale temperature variability during the past two millennia. Nat Geosci, 6: 339-346

Pepin N, Bradley R, Diaz H, Baraër M, Caceres E, Forsythe N, Fowler H, Greenwood G, Hashmi M, Liu X. 2015. Elevation-dependent warming in mountain regions of the world. Nat Clim Chang, 5: 424-430

Rao J, Yu Y, Guo D, Shi C, Chen D, Hu D. 2019. Evaluating the Brewer–Dobson circulation and its responses to ENSO QBO and the solar cycle in different reanalyses. Earth Planet Phys, 3: 166–181

Rienecker M M, Suarez M J, Gelaro R, Todling R, Bacmeister J, Liu E, Bosilovich M G, Schubert S D, Takacs L, Kim G K. 2011. MERRA: NASA's modern-era retrospective analysis for research and applications. J Clim, 24: 3624-3648

Seidel D J, Fu Q, Randel W J, Reichler T J. 2007. Widening of the tropical belt in a changing climate. Nat Geosci, 1: 21-24

Serreze M C, Barry R G. 2011. Processes and Impacts of Arctic Amplification: A Research Synthesis. Glob Planet Change, 77: 85-96

Sexton D M H. 2001. The effect of stratospheric ozone depletion on the phase of the Antarctic Oscillation. Geophys Res Lett, 28: 3697-3700

Shi F, Ge Q, Yang B, Li J, Yang F, Ljungqvist F C, Solomina O, Nakatsuka T, Wang N, Zhao S. 2015. A multi-proxy reconstruction of spatial and temporal variations in Asian summer temperatures over the last millennium. Clim Change, 131: 663-676

Steinman B A, Mann M E, Miller S K. 2015. Atlantic and Pacific multidecadal oscillations and Northern Hemisphere temperatures. Science, 347: 988-991

Stocker T F, Qin D, Plattner G, Tignor M, Allen S, Boschung J, Nauels A, Xia Y, Bex V, Midgley P. 2013. Climate change 2013: the physical science basis Intergovernmental panel on climate change working group I contribution to the IPCC fifth assessment report (AR5). New York: Cambridge University Press

Tang H, Micheels A, Eronen J, Fortelius M. 2011. Regional climate model experiments to investigate the Asian monsoon in the Late Miocene. Clim Past, 7: 847-868

Torrence C, Compo G P. 1998. A practical guide to wavelet analysis. Bull Amer Meteorol Soc, 79: 61-78

van der A, Allaart M, Eskes H. 2015. Extended and refined multi sensor reanalysis of total ozone for the period 1970–2012. Atmos Meas Tech, 8: 3021-3035

Villalba R, Lara A, Masiokas M H, Urrutia R, Luckman B H, Marshall G J, Mundo I A, Christie D A, Cook E R, Neukom R. 2012. Unusual Southern Hemisphere tree growth patterns induced by changes in the Southern Annular Mode. Nat Geosci, 5: 793-798

Wang Z, Zhang X, Guan Z, Sun B, Yang X, Liu C. 2015. An atmospheric origin of the multi-decadal bipolar seesaw. Sci Rep, 5: 8909, doi: 89101038/srep08909

Wei W, Zhang R, Wen M, Kim B J, Nam, J C. 2015. Interannual Variation of the South Asian High and Its Relation with Indian and East Asian Summer Monsoon Rainfall. J Clim, 28: 2623-2634

Wilson R, Cook E, D'Arrigo R, Riedwyl N, Evans M N, Tudhope A, Allan R. 2010. Reconstructing ENSO: the influence of method proxy data climate forcing and teleconnections. J Quat Sci, 25: 62-78

Wu G, Liu Y, Zhang Q, Duan A, Wang T, Wan R, Liu X, Li W, Wang Z, Liang X. 2007. The influence of mechanical and thermal forcing by the Tibetan Plateau on Asian climate. J Hydrometeorol, 8: 770-789

Yao T, Xue Y, Chen D, Chen F, Thompson L, Cui P, Koike T, Lau W M, Lettenmaier D, Mosbrugger V, Zhang R, Xu B, Dozier J, Gillespie T, Gu Y, Kang S, Piao S, Sugimoto S, Ueno K, Wang L, Wang W, Zhang F, Sheng Y, Guo W, Ailikun W, Yang X, Ma Y, Shen S, Su Z, Chen F, Lian S, Liu Y, Singh V, Yang K, Yang D, Zhao X, Qian Y, Zhang Y, Li Q. 2018. Recent Third Pole's rapid warming accompanies cryospheric melt and water cycle intensification and interactions between monsoon and environment: multi-disciplinary approach with observation modeling and analysis. Bull Amer Meteorol Soc

Zhang Y, Zou T, Xue Y. 2019. An Arctic-Tibetan Connection on Subseasonal to Seasonal Time Scale. Geophys Res Lett, 46: doi: 101029/2018GL081476

Zhao P, Yang S, Wang H, Zhang Q. 2011. Interdecadal relationships between the Asian-Pacific Oscillation and summer climate anomalies over Asia North Pacific and North America during a recent 100 years. J Clim, 24: 4793-479

APPENDIX

For

Co-varying temperatures at 200hpa over the three poles

Keyan FANG[1,2,*], Peng ZHANG[2,3], Jingming CHEN[1,4], Deliang CHEN[2]

1. Key Laboratory of Humid Subtropical Eco-geographical Process (Ministry of Education), Fujian Normal University, Fuzhou 350007, China
2. Regional Climate Group, Department of Earth Sciences, University of Gothenburg, Box 460 S-405 30 Gothenburg, Sweden
3. Department of Oceanography, Chonnam National University, 61186 Gwangju, Republic of Korea
4. Department of Geography and Program in Planning, University of Toronto, 100 St. George St., Toronto, Ontario, Canada

Reconstruction of the temperature at 200hpa of the Third Pole

As dating for the ice cores are less accurate than tree rings, we shift the ice cores one year forward and backward when analyzing their linkages with climate as in previous studies (Fang et al., 2018; Neukom et al., 2014). The raw tree-ring measurements were standardized by removing the age-related growth trends fitted by a smoothed cubic spline with a 50% frequency cutoff of 2/3 of the series length (Cook, 1985). The dimensionless tree-ring indices of a site were averaged following a robust biweight mean method (Cook, 1985) to produce the tree-ring chronology. The reliable period of the chronologies were determined when over 6 cores are available as did in previous studies for large-scale reconstructions (Cook et al., 2010; Fang et al., 2010). We only selected the proxies with significant ($p<0.05$) correlation with temperatures at 200hpa for reconstruction. Accordingly, the proxy network was reduced to have 18 proxy series (Fig. S4a and Table S1). The mean length of the selected proxies is 470 years and the longest proxy is 1981 years.

The reconstruction models were verified using a leave-one-out cross-validation procedure (Cook et al., 2010). In application, this method develops a model with one year data out each time, and the model is used to predict the excluded climate data based on the proxy data of that year, which is particularly efficient for the reconstructions with a short common period between a proxy and instrumental data. The cross-validations of the reconstruction suggest its robustness as indicated by above zero value of the Reduction of Error (RE) (0.04) and the sign test (31+/21-).

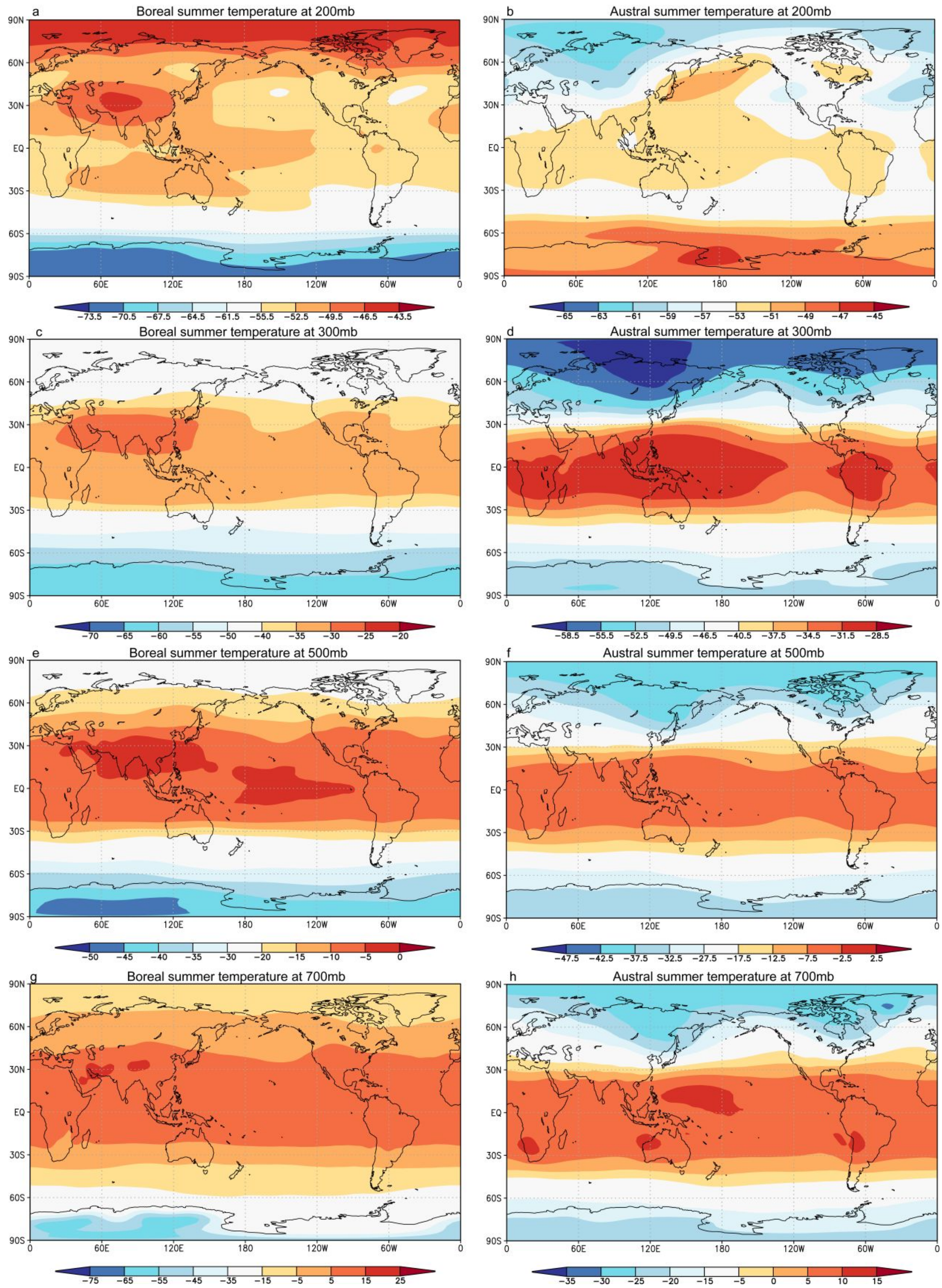

Fig. S1. Mean temperature at (a and b) 200hpa, (c and d) 300hpa, (e and f) 500hpa and (g and h) 700hpa in (a, c, e and g) boreal (June-August) and (b, d, f and h) austral summers (December-February) from the NCEP reanalysis datasets for the period of 1948-2018. Fig. S1a and S1b are similar as the Fig. 1a and 1b except for the contour ranges.

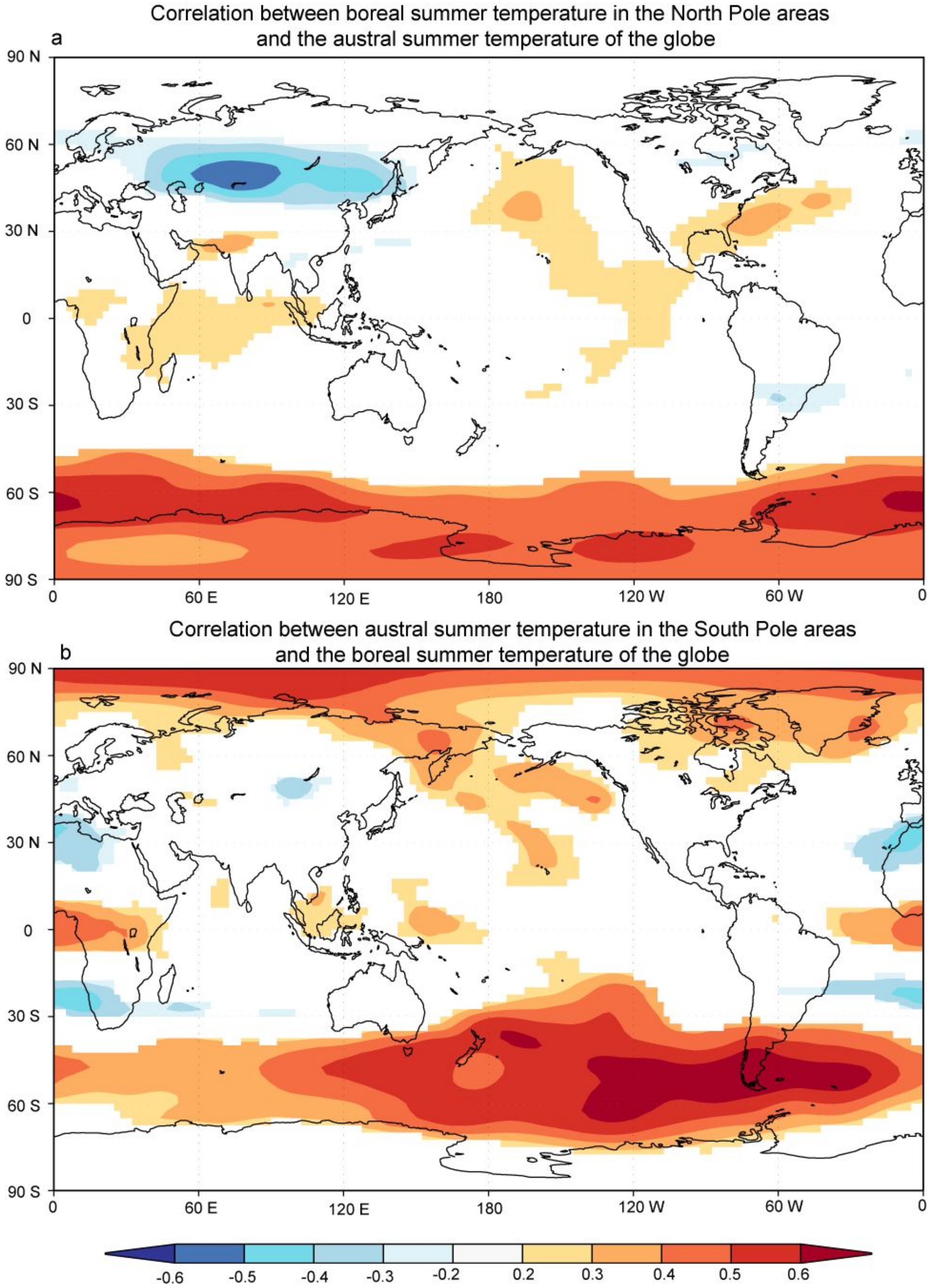

Fig. S2. Map of correlations (a) between the temperature at 200mb in North Pole in boreal summer and the temperature at 200mb of the globe in austral summer, and (b) between the temperature at 200mb in South Pole in austral summer and the temperature at 200mb of the globe in boreal summer.

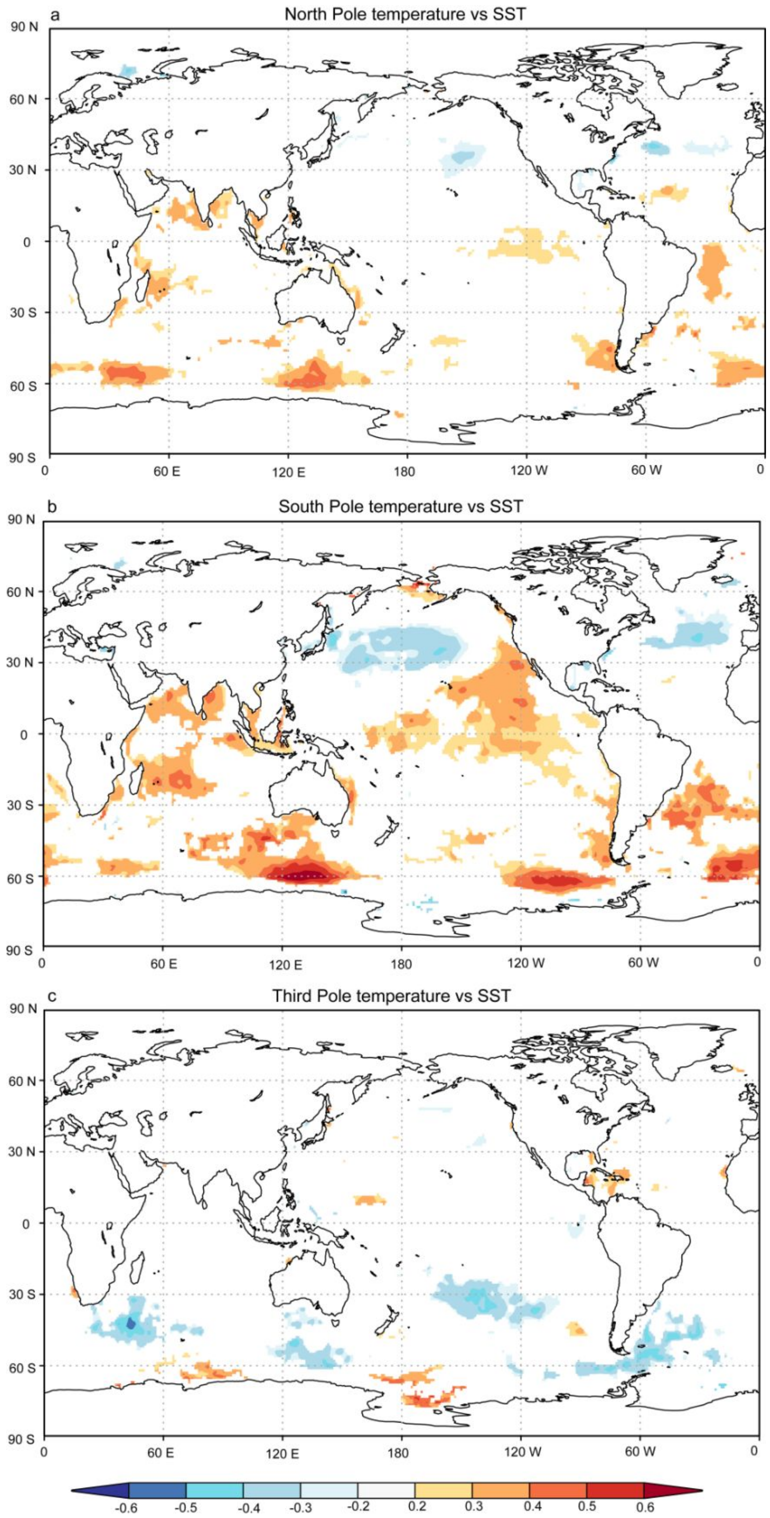

Fig. S3. Map of correlations between the annual sea surface temperature (SST) and the (a) boreal summer temperature at 200hpa in the North Poles, the (b) austral summer temperature at 200hpa among the South Pole and the (c) boreal summer temperature at 200hpa over the Third Pole during their common period 1948-2018.

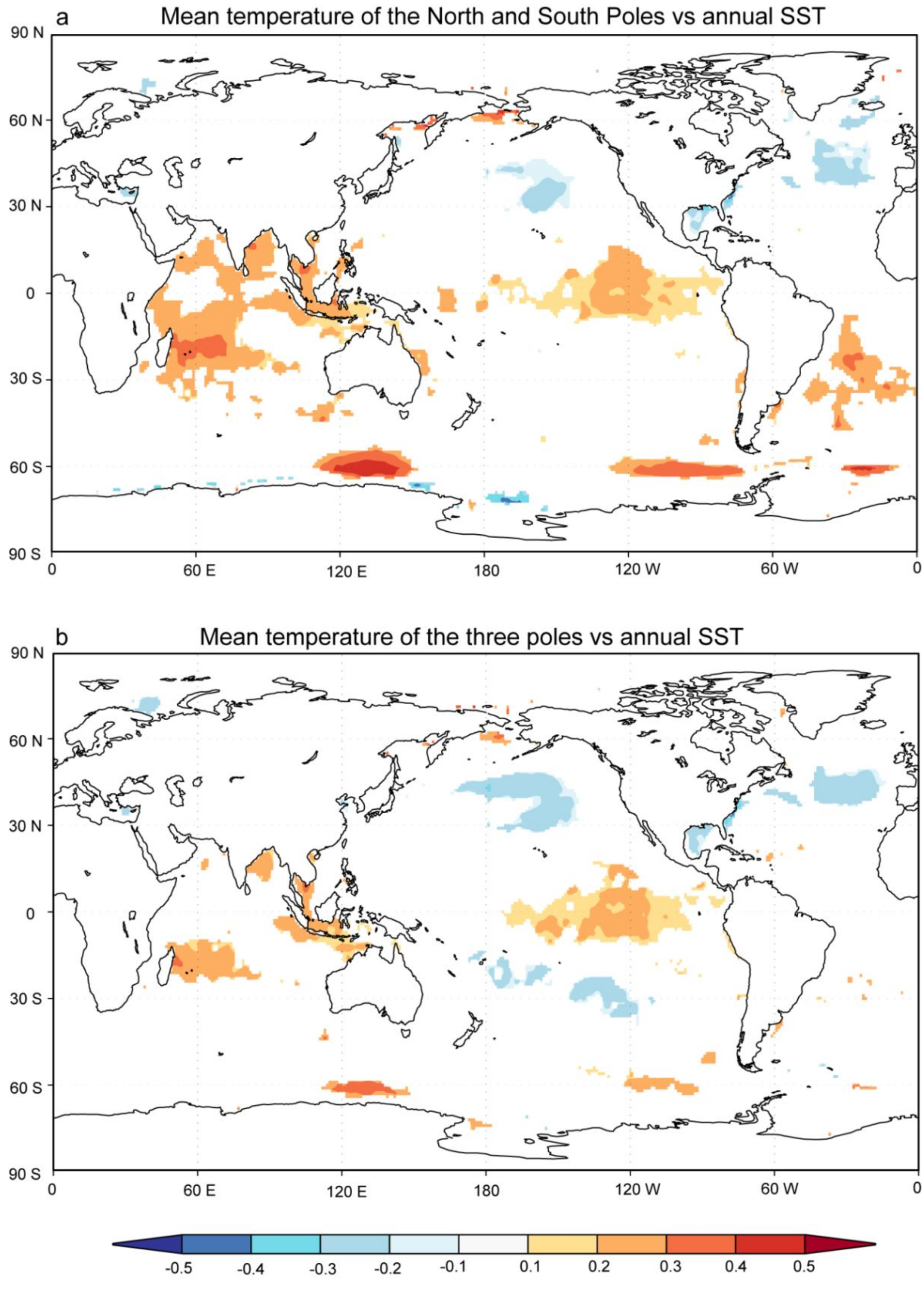

Fig. S4. Map of correlations between the annual sea surface temperature (SST) and the (a) mean summer temperatures at 200hpa of the North and South Poles, the (b) mean summer temperature at 200hpa of the three poles during their common period 1948-2018.

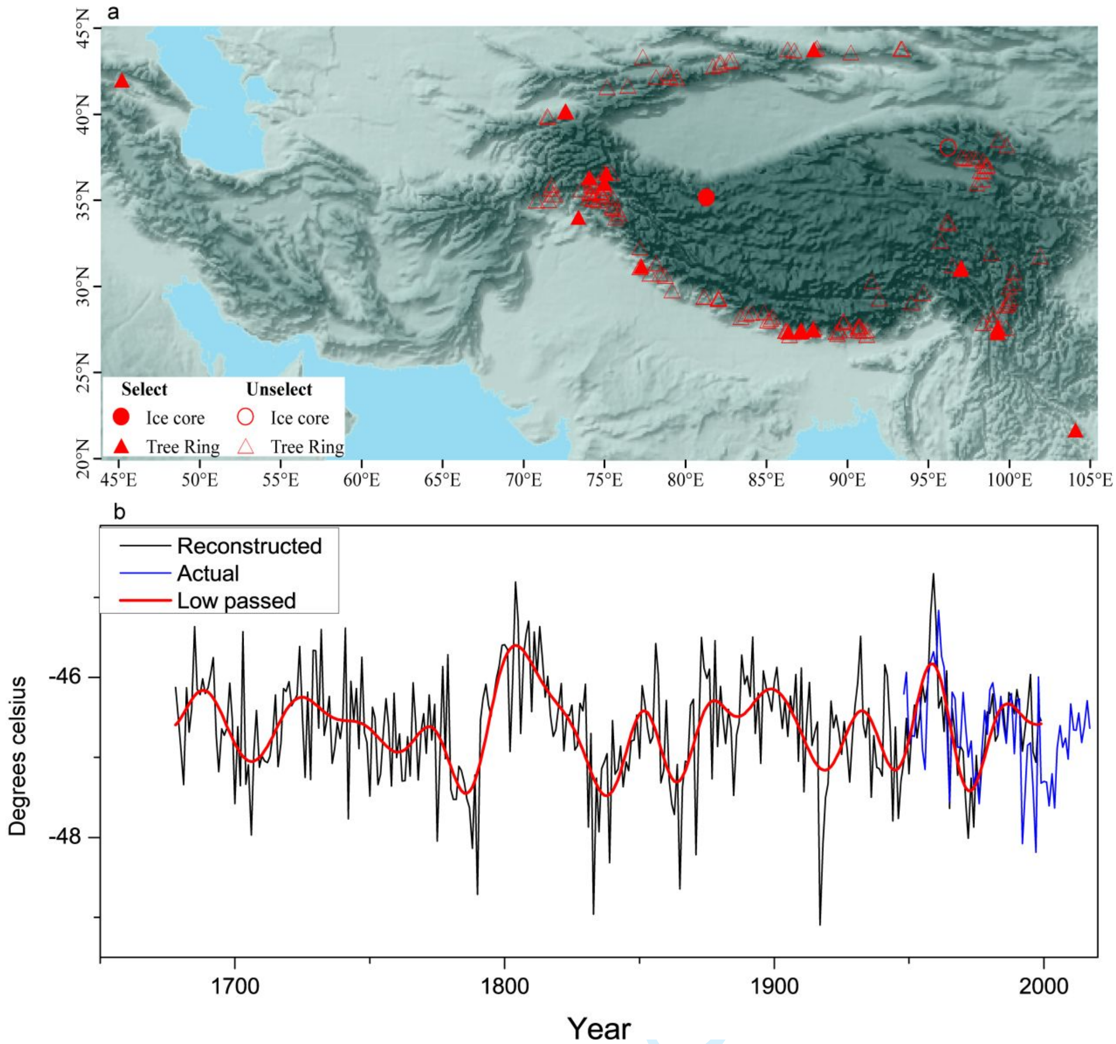

Fig. S5. The (a) locations of the proxy records used for the reconstruction of the temperatures at 200hpa in the Third Poles. The filled symbols are the selected proxies for reconstruction with significant ($p<0.05$) with the climate data. The (b) reconstructed and actual time series of the boreal summer temperatures at 200hpa in the Third Poles and the bold lines indicated the low-passed ($f<0.02$) data.

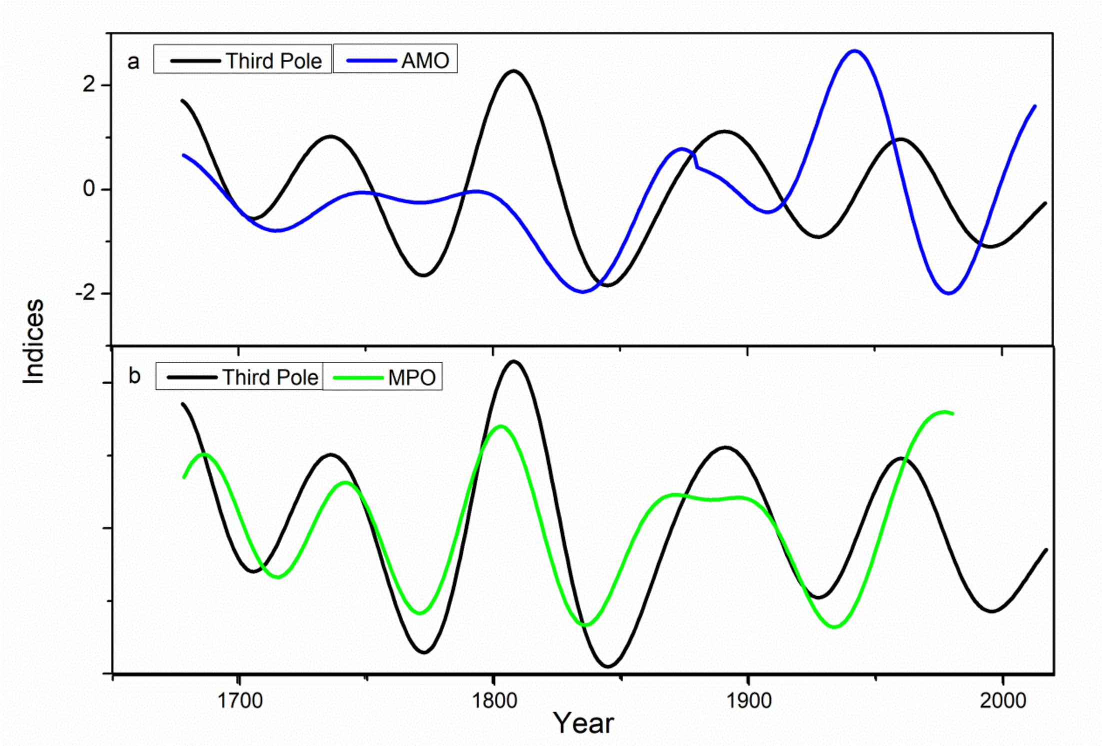

Fig. S6. Comparisons between the reconstructed boreal summer temperature of the Third Pole at 200hpa and the (a) reconstructed Atlantic Multi-decadal Oscillation (AMO), the (b) reconstructed Multi-decadal Pacific Oscillation (MPO). The comparisons were conducted on multi-decadal after low-pass (f<0.02) filtering.

Table S1. Information on the 18 selected proxy records from 202 proxies used for the reconstruction of tropopause temperature in the Third Pole. Locations of the proxies are shown in Fig. 2. Significance level: * = 0.05 and ** = 0.01. TR-W = Tree ring width; IC-O = Ice core d18O.

ID	Site Code	Lat. (N)	Lon. (E)	Proxy	Duration	Corr.	References
1	Guliya	35.17	81.29	IC-O	1602-1987	-.33*	(Thompson et al., 2006)
2	chin025	27.37	99.27	TR-W	1483-2007	-0.28*	(Cook et al., 2010)
3	chin033	43.77	87.92	TR-W	1653-2002	0.30*	(Cook et al., 2010)
4	chin038	27.59	99.29	TR-W	1542-2005	-0.29*	(Fan et al., 2010)
5	chin047	31.12	97.03	TR-W	1406-1994	0.34*	(Bräuning, 1994)
6	chin074	31.00	97.00	TR-W	128-2010	0.25*	(Wang et al., 2014)
7	geor001	42.00	45.17	TR-W	1526-1980	-0.37*	(Cook et al., 2010)
8	indi017	31.18	77.27	TR-W	1673-1989	-0.37*	(Borgaonkar et al., 1999)
9	kyrg002	40.17	72.58	TR-W	1346-1995	0.37**	(Esper et al., 2007)
10	kyrg007	40.17	72.58	TR-W	1157-1995	0.30*	(Esper et al., 2007)
11	nepa027	27.48	87.90	TR-W	1561-1999	-0.27*	(Cook et al., 2010)
12	nepa032	27.40	87.12	TR-W	1546-1996	-0.48**	(Cook et al., 2010)
13	nepa041	27.35	86.35	TR-W	1612-1994	-0.43**	(Cook et al., 2010)
14	paki007	36.33	74.03	TR-W	1141-1993	0.32*	(Esper et al., 2007)
15	paki008	36.00	75.00	TR-W	568-1990	0.53**	(Esper et al., 2007)
16	paki011	36.58	75.08	TR-W	554-1990	0.55**	(Esper et al., 2007)
17	paki032	34.03	73.38	TR-W	1678-2005	-0.30*	(Cook et al., 2010)
18	viet002	21.67	104.10	TR-W	1470-2004	-0.28*	(Buckley et al., 2010)

REFERENCES:

Borgaonkar H P, Pant G B, Kumar K R. 1999. Tree-ring chronologies from western Himalaya and their dendroclimatic potential. IAWA J, 20: 295-309

Bräuning A. 1994. Dendrochronology for the last 1400 years in eastern Tibet. Geosci J, 34: 75-95

Buckley B M, Anchukaitis K J, Penny D, Fletcher R, Cook E, Sano M, Nam C L, Wichienkeeo A, Minh T T, Hong T M, Marcus J. 2010. Climate as a contributing factor in the demise of Angkor Cambodia. Proc Natl Acad Sci U S A, 107: 6748-6752

Cook E, Anchukaitis K J, Buckley B M, D'Arrigo R D, Jacoby G C, Wright W E. 2010. Asian Monsoon Failure and Megadrought During the Last Millennium. Science. 328: 486-489

Cook E. 1985. A time series analysis approach to tree ring standardization. vol PhD. The University of Arizona Tucson USA

Esper J, Frank D C, Wilson R J S, Büntgen U, Treydte K. 2007. Uniform growth trends among central Asian low-and high-elevation juniper tree sites. Trees-Struct Funct, 21: 141-150

Fan Z X, Brauning A, Tian Q H, Yang B, Cao K F. 2010. Tree ring recorded May-August temperature variations since AD 1585 in the Gaoligong Mountains southeastern Tibetan Plateau. Paleogeogr Paleoclimatol Paleoecol, 296: 94-102

Fang K, Chen D, Guo Z, Zhao Y, Frank D, He M, Zhou F, Shi F, Seppä H, Zhang P. 2019. An interdecadal climate dipole between Northeast Asia and Antarctica over the past five centuries. Clim Dyn, 52: 765-775

Fang K, Davi N, Gou X, Chen F, Cook E, Li J, D'Arrigo R. 2010. Spatial drought reconstructions for central High Asia based on tree rings. Clim Dyn, 35: 941-951

Neukom R, Gergis J, Karoly D J, Wanner H, Curran M, Elbert J, González-Rouco F, Linsley B K, Moy A D, Mundo I, Raible C C, Steig E J, Ommen T, Vance T, Villalba R, Zinke J, Frank D. 2014. Inter-hemispheric temperature variability over the past millennium. Nat Clim Chang, 4: 362-367

Tan M, Liu T, Hou J, Qin X, Zhang H, Li T. 2003. Cyclic rapid warming on centennial-scale revealed by a 2650-year stalagmite record of warm season temperature. Geophys Res Let, 30: 1617-1620

Thompson L G, Mosley-Thompson E, Brecher H, Davis M, León B, Les D, Lin P, Mashiotta T, Mountain K. 2006. Abrupt tropical climate change: Past and present. Proc Natl Acad Sci U S A, 103: 10536-10543

Wang J, Bao Y, Qin C, Kang S, He M, Wang Z. 2014. Tree-ring inferred annual mean temperature variations on the southeastern Tibetan Plateau during the last millennium and their relationships with the Atlantic Multidecadal Oscillation. Clim Dyn, 43: 627-640